processes

MDPI

Article

Fracturing Layer Optimization for Gas Hydrate Development Using EDFM Numerical Simulation Method

Qiang Fu [1,2], Mingqiang Chen [1,2,*], Weixin Pang [1,2] and Wei Sun [3]

[1] State Key Laboratory of Offshore Natural Gas Hydrates, Beijing 100028, China
[2] Research Institute of China National Offshore Oil Cooperation, China National Offshore Oil Corporation, Beijing 100028, China
[3] School of Petroleum Engineering, China University of Petroleum (East China), Qingdao 266580, China
* Correspondence: chenmq17@cnooc.com.cn

Abstract

With the increasing global energy demand, natural gas hydrates have become a focus of research and development. The South China Sea deepwater area has abundant natural gas hydrate resources, but its low permeability limits the commercialization process. This paper explores how to enhance gas production from natural gas hydrate reservoirs through a combination of fracturing technology and depressurization using numerical simulations. Numerical experiments were conducted under various well types and fracture configurations to evaluate their effects on cumulative gas production. The fracturing layer was optimized for different well types. We employed the embedded discrete fracture model (EDFM) to characterize the fracture structures in the reservoir and coupled it with a conventional hydrate numerical simulator to simulate different fracture morphologies. The results show that fractures in the three-phase layer provide the most significant production enhancement among all tested layers. Fractures within the three-phase layer deliver the largest production gain among all layers tested. By comparing the development effects of different well types, it is found that the combination of horizontal wells and hydraulic fracturing can effectively improve the recovery of hydrates compared with single well types and traditional exploitation methods. In particular, horizontal wells with stimulated reservoir volume (SRV) yield a big rise in gas production compared with the single-fracture model under identical conditions. Fractures in the three-phase layer shows the most significant improvement in production. Horizontal wells under the three-phase layer achieve about an 88.26% increase in production compared with the single-fracture simulation under the same conditions.

Keywords: natural gas hydrates; embedded discrete fracture model (EDFM); numerical simulation; production enhancement

Check for updates

Academic Editor: Dicho Stratiev

Received: 27 October 2025
Revised: 19 January 2026
Accepted: 20 January 2026
Published: 9 February 2026

Copyright: © 2026 by the authors. Licensee MDPI, Basel, Switzerland. This article is an open access article distributed under the terms and conditions of the Creative Commons Attribution (CC BY) license.

1. Introduction

Ensuring energy security is the core task of energy development. As a major energy consumer in the world, China faces high risks in oil and gas imports and has significant shortcomings in oil and gas resources. China's energy independence needs to be further enhanced [1]. In order to effectively address the issue of global warming, the international community is actively promoting carbon emission reduction. The Paris Agreement aims to control the rise in global average temperature [2]. Under the current framework of the "dual carbon" goals, China is under tremendous pressure to reduce carbon emissions and

urgently needs to accelerate energy technology innovation and build a clean, low-carbon, safe, and efficient energy system. Ice-like crystalline is a compound formed by natural gas molecules and water molecules under high pressure and low temperature conditions [3]. It has a high energy density. After decomposition, 1 m^3 of natural gas hydrate can release about 164 m^3 of natural gas. Compared with traditional energy sources such as coal and oil, its combustion process produces significantly less pollutants [4]. It is estimated that the global natural gas hydrate resources are about 2.1×10^{16} m^3, which is about twice that of other fossil energy sources [5]. Exploration shows that the northern slope of the South China Sea contains extremely rich hydrate resources, with a prospective hydrate resource volume of up to 18.458 billion tons of oil equivalent [6]. The development and utilization of natural gas hydrate resources is of great significance for achieving the dual carbon goals, alleviating China's resource shortages, optimizing the energy structure, and ensuring energy security. The hydrate reservoirs in the South China Sea are typical muddy silt sand reservoirs with low hydrate saturation and poor inherent permeability [7–10], and such characteristics seriously restrict the commercial development and exploitation of natural gas hydrates in the Shenhu sea area.

In 2020, the second round of hydrate production trials was carried out in the Shenhu area. Using the horizontal well depressurization production method, the test sustained gas production for 30 days, achieving a total of 86×10^4 m^3 and an average daily gas production of 2.9×10^4 m^3. Despite this breakthrough, the commercial production of hydrates still requires further technological innovation and optimization [11]. Reservoir stimulation aims to improve the permeability of low-permeability reservoirs by intervening in the near-wellbore area, thereby increasing the local permeability around the production wells [12]. At present, although there is still a lack of cases of reservoir stimulation in actual hydrate reservoir development, researchers have conducted extensive analysis on the feasibility of hydrate reservoir stimulation to evaluate its potential in practical applications. Feng et al. [13] believed that fracturing has a certain effect on increasing natural gas production. Chen et al. [14] found that the cumulative gas production and gas production rate of hydrate reservoirs will be significantly improved after fracturing. Sun et al. studied the effect of horizontal and vertical fractures on gas production enhancement in the Shenhu area of the South China Sea (SH2 site) by analyzing relevant data. They found that horizontal wells combined with hydraulic fracturing technology provided an effective way to enhance natural gas production [15].

In order to improve the gas production potential of hydrate reservoirs, researchers have conducted more research and explored the possibility of using multiple exploitation methods in combination. Studies have shown that the existing single development method struggles to support large-scale long-term commercial development of natural gas hydrates. Therefore, the combined application of multiple mining methods has important research value [16]. Meng [17] simulated the use of dual horizontal wells for depressurization and warm water injection to mine hydrates. Ruan et al. [18] simulated the depressurization combined with a well heating method for natural gas hydrate development at the laboratory scale by numerical simulation. The results show that gas production under the depressurization combined with the well heating development method is better than that under the single depressurization development case. Zhao et al. [19] evaluated the production performance of the low-frequency electric heating-assisted depressurization (LF-EHAD) method for hydrate sediment recovery. The results showed that LF-EHAD outperforms hot water injection with the same heat injection, offering higher gas production, better energy efficiency, and lower water production. According to the second trial production report in China, the permeability of sediments ranges from 2.38×10^{-3} μm^2 to 6.8×10^{-3} μm^2 [20]. Studies have shown that the pressure and heat transfer effects in low-permeability hydrate

reservoirs are limited, which slows down the advancement of the hydrate decomposition front. It is often difficult to achieve commercial production levels solely by joint production methods, and other methods must be combined. Therefore, it is critical to construct a suitable fracture characterization model. Hydraulic fracturing is a technique that induces the formation, expansion, and merging of microcracks in underground reservoirs by applying continuous hydraulic pressure [21]. Ito et al. [22] conducted an experiment in sediments without hydrates, where fluid injection induced fracture-like structures at the boundary between the sand and clay layers. Zhang et al. [23] conducted a series of triaxial hydraulic fracturing experiments on highly saturated methane hydrate-bearing sand (MHBS) samples to explore the effect of different fluid viscosities on fracture formation. Researchers introduced discrete fracture models (DFMs) and embedded discrete fracture models (EDFMs) to characterize fracture structures more accurately. Karimi-Fard [24] used a discrete fracture model to numerically simulate fracture media with capillary pressure. Lee's research group [25] and Moinfar et al. [26] proposed an embedded discrete fracture model.

The discrete fracture model (DFM) is a numerical method that represents the fracture as a one-dimensional entity and combines it with the matrix part to accurately simulate the effect of the fracture on fluid flow. Carlson et al. [27] compared the applicability of DFM and the dual-porosity medium model. The study showed that when the fracture spacing is large, the simulation accuracy of the dual-porosity medium model decreases significantly, while DFM still maintains a high accuracy. Karimi-Fard et al. [28] proposed and developed a discrete fracture model (DFM) to simulate the flow of fluid in fractured media by simplifying the fracture into a one-dimensional entity. The embedded discrete fracture model (EDFM) is a numerical method that simulates fractures by embedding them into the matrix as source and sink terms. Compared with DFM, the biggest advantage of EDFM is that it simplifies the modeling process of fracture geometry. Lee et al. [29] proposed an embedded discrete fracture model (EDFM). Moinfar et al. [30] extended the embedded discrete fracture model (EDFM) to three dimensions for low-permeability reservoirs and developed a proprietary reservoir simulator, accurately modeling and improving the production efficiency of low-permeability reservoirs. Tene et al. [31] proposed a projection-based embedded discrete fracture model (pEDFM). In numerical experiments under both single phase and multiphase flow conditions, pEDFM demonstrated higher simulation accuracy than the original EDFM, proving its superiority in simulating fluid flow in naturally fractured reservoirs. Jiang et al. [32] benchmarked the performance of the improved pEDFM method under multiphase flow conditions by designing multiple test cases with different fracture geometries and performed a mesh convergence analysis. In summary, EDFM, as an effective fracture characterization method, has been successfully applied in the numerical simulation of many complex fracture networks. Compared with the traditional simplified fracture model, EDFM can more accurately describe the geometric morphology and fluid flow characteristics of fractures, and is particularly suitable for simulations under complex fracture and hydraulic fracturing conditions. By now, only a few studies have used the EDFM in gas hydrate development simulation.

This study aims to develop a coupled simulation framework that integrates the embedded discrete fracture model (EDFM) with hydrate reservoir simulators, enabling a more accurate representation of complex fracture networks and their influence on fluid flow. It further analyzes the enhancement effects of various fracture geometries and well configurations including vertical, horizontal, and multilateral wells on gas production performance in hydrate-bearing sediments. Based on field-inspired geological models, the study also seeks to optimize fracture placement and reservoir stimulation strategies, with the ultimate goal of improving production efficiency and providing theoretical and technical support for the efficient development of natural gas hydrate resources.

The findings of this study are expected to provide practical insights for the commercial exploitation of gas hydrates in complex deepwater environments. By improving the understanding of fracture behavior and optimizing well–fracture configurations, this work offers applicable technical solutions for enhancing gas recovery from low-permeability hydrate reservoirs. These contributions are particularly valuable for advancing hydrate development in regions like the South China Sea, where geological conditions present significant production challenges.

2. Numerical Simulation of Hydrate Reservoir Production Enhancement Based on Embedded Discrete Fractures

This part aims to establish a new method for characterizing fractures in hydrate reservoir fracturing by coupling EDFM with conventional hydrate numerical simulators, and to verify the model for different fracture morphologies and different reservoir physical fields to illustrate the feasibility of coupling, laying the foundation for subsequent research.

2.1. Numerical Simulation Model for Hydrate Reservoir Development

In this study, the complex processes occurring in the hydrate reservoir were realized by modifying the mature hydrate simulator CMG-STRAS and the hydrate phase was regarded as a solid phase component. The results of many researchers have verified the feasibility of this model. The NNC should be defined in the CMG-STARS.

The construction of the hydrate reservoir development numerical simulation model (hereinafter referred to as the development model) includes the hydrate decomposition kinetic equation, mass conservation equation, and energy conservation equation. The development model is a three-phase, three-component model, in which the three phases are the water phase, the gas phase, and the hydrate phase, and the three components are methane gas, water, and natural gas hydrate. In order to facilitate the establishment of the model, the following reasonable assumptions are adopted:

(1) The only gas produced by the decomposition of natural gas hydrate is methane;
(2) The occurrence of a hydrate decomposition reaction will lead to changes in formation porosity;
(3) The flow of liquid and gas in the pores conforms to Darcy's flow law;
(4) Hydrates are evenly distributed in the reservoir;
(5) The solubility of methane in water is not considered.

2.1.1. Hydrate Decomposition Kinetic Equation

In this paper, the decomposition and generation of natural gas hydrates are regarded as the chemical reaction between methane and water, which is expressed by Formula (1):

$$CH_4(g) + nH_2O(l) \Leftrightarrow CH_4 \cdot nH_2O(s) \quad (1)$$

where n is the hydration number related to the hydrate structure and is dimensionless; g, l, and s represent the gas, liquid, and solid three-phase states, respectively. Based on the research results, n = 5.75 is taken in this paper. In this paper, the Kim–Bishnoi kinetic equation is used to describe the decomposition of natural gas hydrates. The driving force for hydrate decomposition is considered to be the gas fugacity difference between the three-phase equilibrium and the gas phase pressure, which is expressed as follows [33,34]:

$$\frac{dc_h}{dt} = k_d A_d (p_e - p_g) \quad (2)$$

where c_h is the hydrate solid phase concentration, gmole/m^3; k_d is the hydrate decomposition rate constant, gmole/(d·kPa·m^2); A_d is the hydrate surface area per unit volume, m^2/m^3; p_e is the phase equilibrium pressure, kPa; p_g is the gas phase pressure, kPa.

Transform $(p_e - p_g)$ into $p_e(1 - p_e/p_g)$, define p_e/p_g as $1/K(p,t)$, and let p_e be

$$p_e = \frac{y_i p_g}{x_i} \tag{3}$$

where y_i and x_i are the mole fractions of methane in the gas and liquid phases, dimensionless; $K(p,t)$ is the hydrate phase equilibrium value at a certain pressure and temperature, dimensionless. Assume a three-phase system of liquid water, hydrate, and methane gas $x_i = 1$.

Substituting Equation (3), k_d, and A_d into Equation (2), the hydrate decomposition kinetic equation becomes [33,34]

$$\frac{dc_h}{dt} = \left(\frac{k_d^0 A_{HS}}{\rho_w \rho_h}\right)(\varphi S_w \rho_w)(\varphi S_h \rho_h)(y_i p_g)\left(1 - \frac{1}{K(p,T)}\right)\exp\left(-\frac{E}{RT}\right) \tag{4}$$

where ρ_w and ρ_h are the densities of water and hydrate, kg/m^3. The mass transfer coefficient is defined as λ_d. Then Formula (4) becomes

$$\frac{dc_h}{dt} = \lambda_d(\varphi S_w \rho_w)(\varphi S_h \rho_h)(y_i p_g)\left(1 - \frac{1}{K(p,T)}\right)\exp\left(-\frac{E}{RT}\right) \tag{5}$$

2.1.2. Mass Conservation Equation

The hydrate decomposition reaction follows the law of conservation of mass. The basic relationship equation of the law of conservation of mass can be expressed as [33,34]

$$\frac{\partial(\varphi \rho_g S_g)}{\partial t} = \nabla \cdot (\rho_g v_g) + \dot{m_g} + q_g \tag{6}$$

$$\frac{\partial(\varphi \rho_w S_w)}{\partial t} = \nabla \cdot (\rho_w v_w) + \dot{m_w} + q_w \tag{7}$$

$$\frac{\partial(\varphi \rho_h S_h)}{\partial t} = \dot{m_h} \tag{8}$$

where v_g and v_w are the flow rates of methane gas and liquid water, m/s; ρ_g is the density of methane gas, kg/m^3; S_g is the gas saturation, dimensionless; $\dot{m}_g$, $\dot{m}_w$, and $\dot{m}_h$ are the mass changes in each component, kg/(m^3·s); q_g and q_w are the gas production rate and water production rate of the well, m^3/s.

2.1.3. Energy Conservation Equation

The hydrate decomposition reaction also follows the law of conservation of energy. The basic relationship equation of the law of conservation of energy can be expressed as [33,34]

$$\begin{aligned} &\nabla \cdot (\lambda_c \nabla T) - \nabla \cdot \left(\rho_g v_{gr} H_g + \rho_w v_{wr} H_w\right) + q_g H_g + q_w H_w + Q_h = \\ &\tfrac{\partial}{\partial t}\left[(1-\varphi)\rho_s H_s + \varphi(\rho_h S_h H_h + \rho_w S_w H_w + \rho_g S_g H_g\right] \end{aligned} \tag{9}$$

where Q_h is the energy required for hydrate decomposition provided by the outside world, J/(m^3·s); H_g, H_w, H_h, and H_s are the enthalpies of gas, water, hydrate, and rock skeleton, J/mole; ρ_s is the rock density, kg/m^3; λ_c is the effective thermal conductivity of sediment, J/(m·s·K).

2.2. Embedded Discrete Fracture Model

This study uses an embedded discrete fracture model (EDFM) to characterize hydraulic fractures in hydrate reservoirs. The embedded discrete fracture model discretizes fractures into fracture segments of different shapes and sizes through the matrix grid boundary, and uses additional grids to represent the fracture units in the original physical model. The mass transfer between fractures and matrix is achieved by establishing a connection between fracture units and matrix units, avoiding the generation of too many encrypted grids in the simulation of complex fractures with different geometric shapes.

This paper mainly focuses on the influence of plane fracture complexity on gas production and the evolution of the seepage field. In order to reduce the difficulty of fracture morphology construction, the simulation of hydraulic fractures adopts the following assumptions:

(1) The reservoir is considered to be a rock with isotropic and homogeneous permeability;
(2) The fracture network is distributed in a planar manner and does not deflect in the longitudinal direction;
(3) The two-point flux approximation format is used to connect adjacent fracture segments in the discrete computational domain;
(4) Mass transfer between intersecting fracture segments is approximated by the distribution transfer coefficient;
(5) In a single matrix grid, the fracture is assumed to completely penetrate the grid in the vertical direction.

The non-neighborhood connection (NNC) T_{NNC} in the embedded discrete fracture model is

$$T_{\mathrm{NNC}} = \frac{k_{\mathrm{NNC}} \cdot A_{\mathrm{NNC}}}{d_{\mathrm{NNC}}} \tag{10}$$

where k_{NNC} is the permeability in the NNC connection, 10^{-3} μm^2; A_{NNC} is the contact area, m^2; d_{NNC} is the characteristic distance, m.

NNC types can be divided into three categories. The first category is the connection between the fracture segment and the matrix grid it penetrates.

The conductivity of the fracture grid between individual fracture segments is considered the second type of NNC, and the conductivity coefficient is described by the two-point flow approximation method.

The connection between intersecting fracture segments is considered the third type of NNC. A conductivity coefficient is set at the intersection of fracture segments to approximate the mass exchange of fracture intersections.

Taking into account the situation where fractures intersect the wellbore, the well index (WI) is calculated as follows:

$$WI = \frac{2\pi k_{\mathrm{f}} w_{\mathrm{f}}}{\ln(\frac{r_{\mathrm{e}}}{r_{\mathrm{w}}})} \tag{11}$$

$$r_{\mathrm{e}} = 0.14\sqrt{L_{\mathrm{s}}^2 + H_{\mathrm{s}}^2} \tag{12}$$

where L_{s} is the length of the fracture segment, m; H_{s} is the height of the fracture segment, m; r_{e} is the effective radius, m; r_{w} is the wellbore radius, m.

In the calculation of EDFM [35,36], the characteristic distance of the first type of d_{NNC} NNC can be simplified by the geometric relationship between the grid and the crack surface. Tene et al. [31] proposed four geometric algorithms for the characteristic distance of the first type of connection, namely the expression for the case where the fracture crosses the grid—that is, the crack is perpendicular to the grid boundary—and the case where the fracture crosses the grid diagonal d_{NNC}.

In this study, since the cracks were reduced in dimension, the deflection of the cracks in the vertical direction of the matrix grid was not considered. Therefore, the matrix grid was divided into rectangles and triangles, and the characteristic distance was simplified to the weighted average value from the centroid of each part to the centroid of the fracture segment, which is

$$d_{\mathrm{NNC}} = \frac{\mathrm{d}_1 \cdot S_1 + \mathrm{d}_2 \cdot S_2 + \mathrm{d}_3 \cdot S_3 + \mathrm{d}_4 \cdot S_4}{S_1 + S_2 + S_3 + S_4} \tag{13}$$

where d_1, d_2, d_3, and d_4 are the distances from the centroid of each part to the centroid of the fracture segment in the matrix grid, m; S_1, S_2, S_3, and S_4 are the areas of each part, m^2.

In particular, as shown in Figure 1, the specific implementation steps of EDFM are as follows:

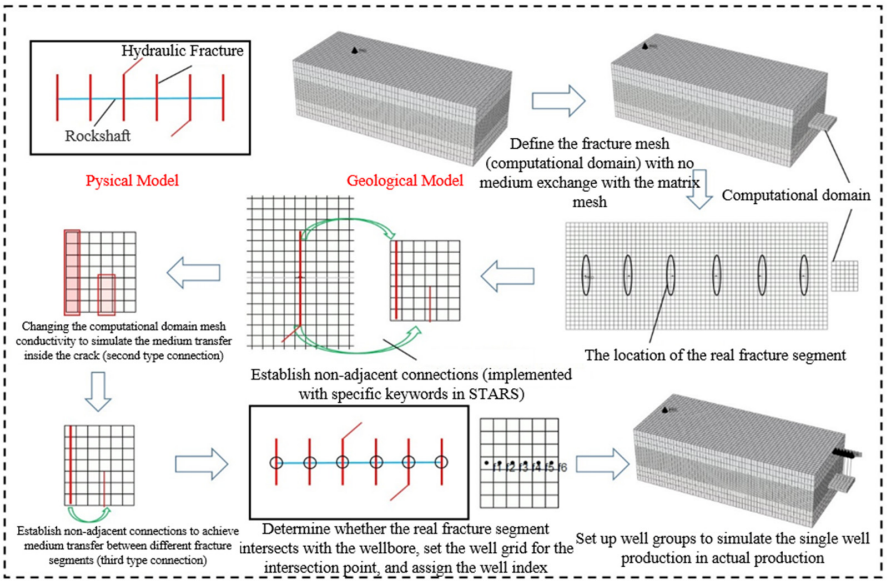

Figure 1. Schematic diagram of the EDFM realization process.

After all NNCs are defined, the CMG simulator is called and performed. The fully implicit method is used to solve the whole model.

3. Simulation of Hydrate Reservoir Production Enhancement Considering Simple Hydraulic Fractures

This section carries out a numerical simulation study on hydraulic fracturing-assisted pressure reduction development in Class III hydrate reservoirs based on EDFM. Two types of fracture simulation methods were set up, namely considering only a single double-wing morphological fracture and considering the reservoir transformation volume around the fracture. On this basis, the impact of fracture conductivity, fracture length, and fracture number on the production increase effect of different simulation methods and different well types was analyzed, and the characteristics of physical field changes under the influence of different parameters were clarified.

In order to study the effect of fractures on hydrate decomposition behavior, a Class III hydrate reservoir model was constructed based on the geological parameters of the hydrate-bearing layer (HBL) in the Shenhu area of the South China Sea. Table 1 gives the parameter values used. The physical model size in the vertical well and multilateral well cases in this section was 220 m × 220 m × 96 m, and the grid division used was 44 × 44 × 24; the physical model size in the horizontal well case was 300 m × 125 m × 96 m, and the grid division was 60 × 25 × 24. The settings of vertical wells, horizontal wells, and multilateral wells and the distribution of fractures are shown in Figure 2.

Table 1. Parameters used in the physical model.

Parameter Name	Numeric
Bottom hole pressure/kPa	4500
Rock density/(kg·m^{-3})	2650
Matrix permeability/10^{-3} μm^2	2.9
Hydrate saturation	0.34
Reservoir porosity	0.35
Hydrate thermal conductivity/(J·m^{-1} d^{-1} K^{-1})	3.395×10^4
Thermal conductivity of water/(J·m^{-1} d^{-1}·K^{-1})	5.183×10^4
Thermal conductivity of gas/(J·m^{-1}·d^{-1} K^{-1})	1.4×10^2
Geothermal gradient/(°C km^{-1})	48
Immune water saturation	0.3
Bound gas saturation	0.03
Water permeability reduction index	5.0
Gas permeability reduction index	3.5
Initial value of capillary pressure/Pa	1×10^5

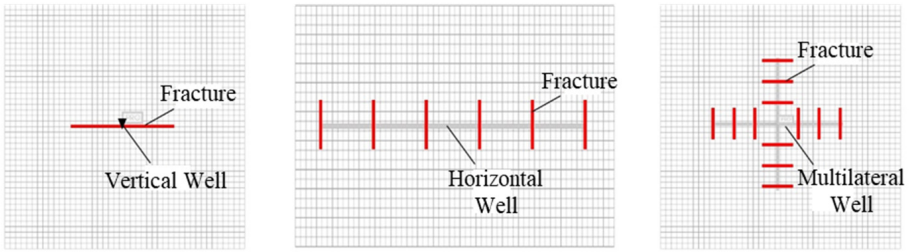

(a) Fracture Arrangement in Vertical Well Production (b) Fracture Arrangement in Horizontal Well Production (c) Fracture Arrangement in Multilateral Well Production

Figure 2. Schematic diagram of fracture distribution.

In this work, the following boundary conditions were applied in the numerical simulations: all lateral boundaries were set as no-flow ones to ensure mass conservation within the reservoir domain; the top and bottom boundaries were defined as adiabatic, preventing heat exchange. The production well was modeled as a constant pressure sink with a bottom hole pressure of 4500 kPa to simulate depressurization. Temperature boundaries were determined using a geothermal gradient of 0.051 °C/m, consistent with field conditions in the Shenhu area.

To enhance simulation accuracy, locally refined grids were applied near the wellbore to better capture pressure and saturation gradients. A mesh sensitivity analysis was conducted, and further grid refinement resulted in less than 2% change in cumulative gas production, indicating that the current grid configuration achieves sufficient numerical stability and convergence for engineering purposes.

4. On-Site Case Analysis

In order to study the field application of the fracture simulation method, this section constructs a numerical simulation model of hydraulic fracturing-assisted depressurization production of different well types based on the geological data of the first test production, analyzes the production increase effect brought by the arrangement of fractures in different layers, and explores the influence of single fractures (double-wing fracture type) and fractures considering SRV (stimulated reservoir volume) on the actual reservoir. SRV is a critical parameter in evaluating the effectiveness of hydraulic fracturing in unconventional reservoirs, representing the volume of rock that has been effectively stimulated to enhance hydrocarbon production. In the simulations, the SRV was conceptually represented as

a region surrounding the main hydraulic fractures and was numerically implemented by applying a significant permeability multiplier to the matrix grids within this defined volume. This is a simplified approach to simulate the enhanced flow capacity of the stimulated zone.

4.1. History Matching of Test Model

According to the characteristics of the hydrate reservoir in the Shenhu sea area, an idealized rectangular hydrate reservoir model was constructed to simulate the exploitation of the hydrate reservoir. The model was 560 m long, 560 m wide, and 157 m high. The grid was set to 56 × 56 × 24, where the grids in the z direction were divided into 4, 5, 5, 6, and 4. The thicknesses of the upper cap layer, hydrate layer (HBL), three-phase layer (TPL), free gas layer (FGL), and lower cap layer in the model were 40 m, 35 m, 15 m, 27 m, and 40 m, respectively. The temperature of each hydrate layer was calculated based on the geothermal gradient of 0.051 °C/m. During the history matching, the vertical well production was set to penetrate the three-phase layer (model layers 10–14) because the three-phase layer was the exploitation layer for trial exploitation. Since the report did not provide the gas saturation data of the three-phase layer, it was set to 0.18 based on the fitting results. The specific parameters of the model are shown in Table 2. As the experiment cannot create a real scale fracture, a field scale study is performed. The test data in Shenhu sea area is utilized. Taking into account the increase in reservoir permeability and free gas saturation near the wellbore caused by drilling, the gas saturation (0.40) and permeability (5.7×10^{-3} μm^2) of the grid near the wellbore were adjusted to achieve the fitting effect. The fitting results are shown in Figure 3. The fitting results achieved over 90% accuracy. On this basis, the hydraulic fracture is set to the formation to analyze its effect.

Table 2. Fundamental geological parameters of each layer.

Parameter	Hydrate Layer	Three-Phase Layer	Water Layer
Thickness/m	35	15	27
Porosity	0.35	0.33	0.32
Permeability/10^{-3} μm^2	2.9	1.5	7.4
Water saturation	0.66	0.51	0.922
Gas saturation	0	0.18	0.078
Hydrate saturation	0.34	0.31	0

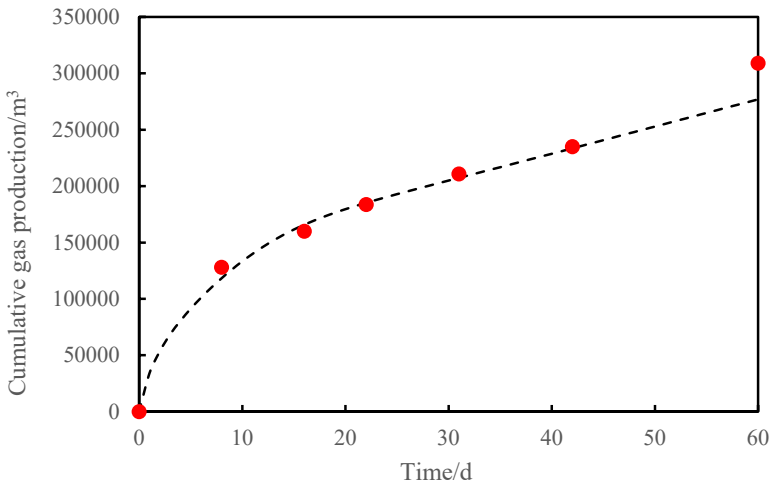

Figure 3. Comparison of simulation results with 2017 test production results in SCS (curve: fitting data; dot: real data).

4.2. Optimal Vertical Well Fracturing Position

In this section, the optimized fracture location in vertical well fracturing production is explored by setting fractures in different layers. A total of seven groups of simulation results were compared, including single-layer fracturing production, double-layer fracturing production, and three-layer fracturing production. The schematic diagram of the fracture arrangement is shown in Figure 2. In these simulation cases, the fracture length was set to 50 m, the conductivity was 100×10^{-3} μm^2·m (the conductivity can be changed depending on the in situ stress and fracturing parameters), and the fracture was set to penetrate the layer in the vertical direction. The specific simulation categories are shown in Table 3.

Table 3. Simulation groups of different fracture locations in the vertical well case.

Simulation Groups	Fracture Placement Layers
SH-V-1	HBL (hydrate-bearing layer)
SH-V-2	TPL (three phases layer)
SH-V-3	FGL (free gas layer)
SH-V-4	HBL + TPL
SH-V-5	HBL + FGL
SH-V-6	TPL + FGL
SH-V-7	HBL + TPL + FGL

Figure 4 shows the cumulative gas production curve of 3000 days of simulation under single layer simulation. Overall, among the seven simulation cases, SH-V-2 had the lowest final cumulative production, which was 1.743×10^7 m^3, and SH-V-7 had the highest cumulative yield, which was 3.321×10^7 m^3. Overall, the cumulative production showed an increasing trend with the increase in the longitudinal height (LH) of the fracture; however, production did not scale linearly with fracture height (LH), as SH-V-4 and SH-V-6 showed similar outputs. Well location also played a key role; however, fracture height (LH) showed no linear relationship with production, as indicated by the similar outputs of SH-V-4 and SH-V-6, which showed that the location of the fracturing well was also one of the factors affecting the production.

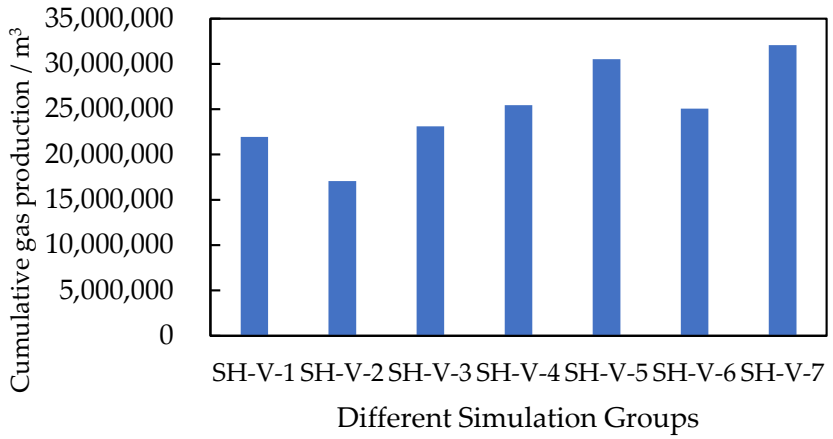

Figure 4. Cumulative gas production under different simulation cases.

Figure 5 shows the gas/water ratio curve. It can be found that the change in the gas/water ratio can be divided into two stages: In the first stage, the gas/water ratio rose rapidly to a peak value and then decreased. Since a high free gas saturation was set at the wellbore, the peak value can often reach thousands or even tens of thousands. However, since this stage was often less than 1 to 2 days before production, it is not discussed in detail.

Only the image of the second stage is taken as the basis for discussion. In the second stage, the gas/water ratio gradually rose after stable production. Combined with the change in the gas/water ratio in this stage, it was not difficult to find that, in the single-layer fracturing case simulated by a single fracture, FGL had the highest cumulative production, while TPL had the worst production increase effect. This was also reflected in the case of double-layer fracturing. Specifically, the gas production of SH-V-5 was always higher than that of SH-V-4, and the production and the gas/water ratio of SH-V-5 were close to those of SH-V-7 of three-layer fracturing. This shows that, under the condition that only one fracture can be formed at a single perforation point, the production potential is greater when FGL is selected as the location of the fracturing well.

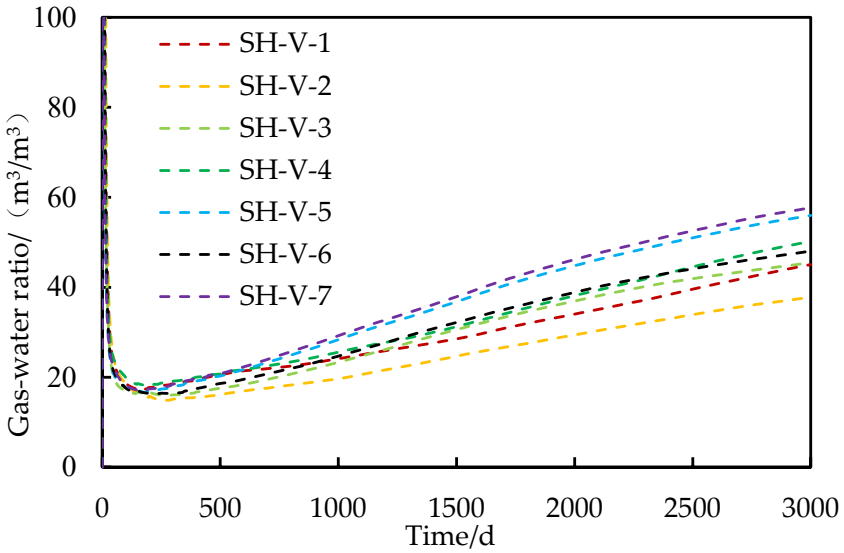

Figure 5. Gas-to-water ratio curves under different simulation cases.

Figure 6 shows the cumulative gas production curve under SRV simulation. Different from the single layer simulation, the cumulative production of FGL under SRV simulation was 2.526 × 10^7 m^3, the gap with TPL narrowed, and it no longer had an advantage. HBL became the layer with the greatest gas production potential, with a cumulative production of 2.988 × 10^7 m^3, and the output increased by about 34.05% compared with the single-slit simulation.

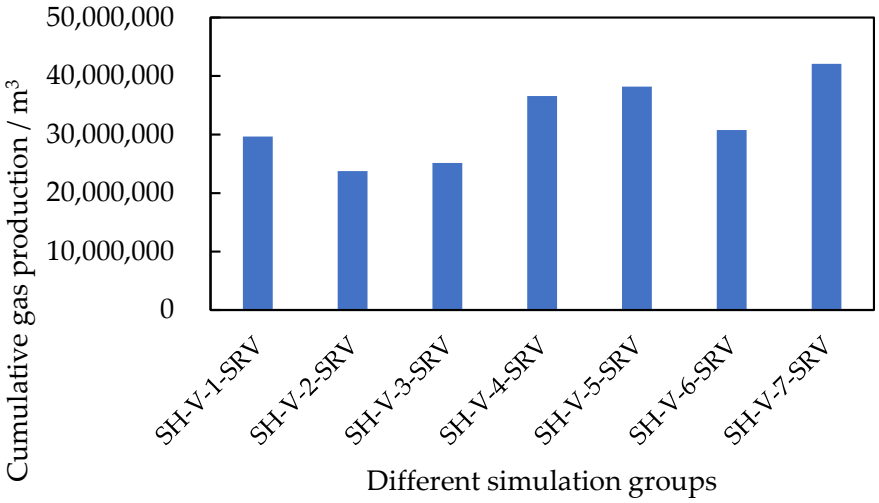

Figure 6. Cumulative gas production considering the SRV simulation approach.

Figure 7 describes the gas/water ratio curve under SRV simulation. It can be seen that the gas/water ratio of HBL was 55.58 m^3/m^3 at 3000 days, which exceeded the SH-V-6 of double-layer fracturing. Similarly, compared with the single-fracture simulation, SH-V-4 significantly improved, and the gas/water ratio curves of TPL and FGL were close, which shows that the production increase effect of TPL also significantly improved.

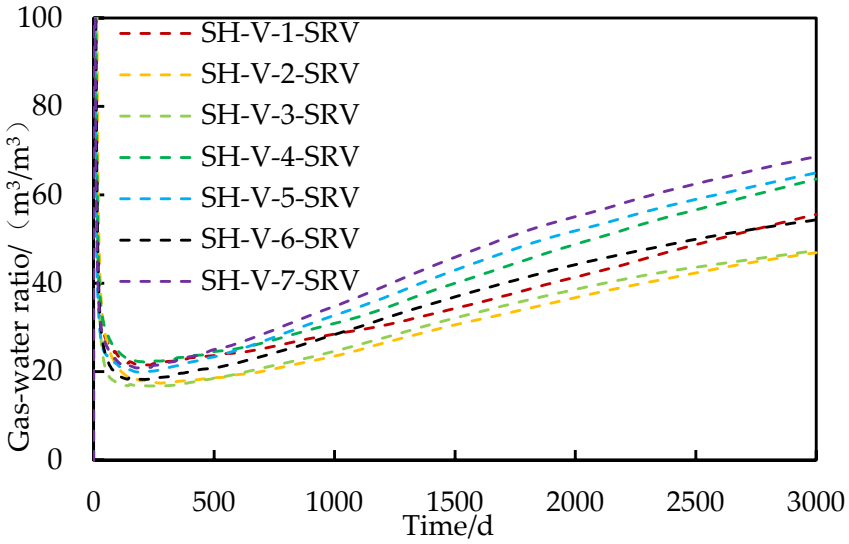

Figure 7. Gas-to-water ratio curves considering the SRV simulation approach.

4.3. Optimal Horizontal Well Fracturing Position

This section explores the effect of the arrangement of multi-stage fracturing horizontal wells in each layer on the production increase effect. The perforation position and fracture setting of the horizontal wells are similar to those in Figure 2, where the number of fractures was 5, the fracture spacing was 100 m, the fracture half-length was 50 m, and the fracture conductivity was 100 × 10^{-3} μm^2 m. The multi-stage fracturing horizontal wells were arranged in HBL, TPL, and FGL, and the fractures were set vertically to run through the entire layer where the horizontal wells were located.

Figure 8 describes the cumulative gas production curves of multi-stage fracturing horizontal wells arranged in different layers. HBL achieved the maximum cumulative production, which was 4.861 × 10^7 m^3; the final gas production of the one arranged at FGL was the lowest, which was 2.527 × 10^7 m^3; and the production of SH-H-HBL increased by about 92.36% compared with SH-H-FGL. The reason for this is that the perforation points and hydraulic fractures are all arranged in the horizontal section. Due to the low permeability of the reservoir, the multi-stage fracturing horizontal wells arranged in FGL cannot smoothly transmit the pressure drop to HBL and TPL during the pressure reduction production process, resulting in a low hydrate decomposition rate in these two layers, and the fluid produced by the decomposition cannot be transported to the wellbore in time. In general, compared with vertical wells, multi-stage fracturing horizontal wells have greater production advantages.

Figure 9 shows the curve of the change of the gas/water ratio over time. TPL and FGL still conformed to the two stages of the change in the gas/water ratio in vertical wells. However, when the horizontal well section was arranged at HBL, the slope of the gas/water ratio curve became gentle at about 900 days, and the slope of the curve increased again at about 2000 days. Combined with the cumulative production curve, it was not difficult to infer that the water production increased in the middle of production and tended to be stable in the later period, so the rate of increase in the gas/water ratio accelerated. At 3000 days, the gas/water ratios of the three simulation groups were 82.23 m^3/m^3,

57.13 m^3/m^3, and 42.37 m^3/m^3, respectively. It can be judged that, when a multi-stage fracturing horizontal well is used and a single perforation point can only form one fracture, selecting HBL as the location of the fracturing well has the best production increase effect.

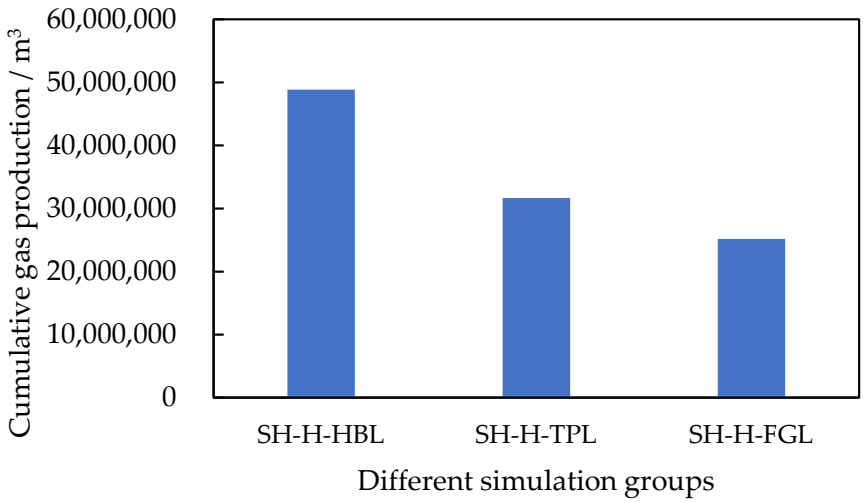

Figure 8. Cumulative gas production under different simulation cases.

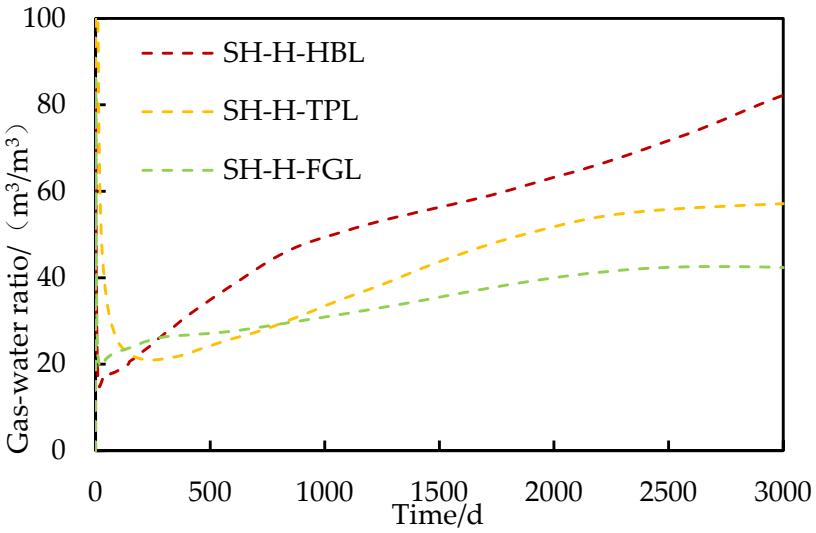

Figure 9. Gas-to-water ratio curves under different simulation cases.

Figures 10 and 11, respectively, describe the cumulative gas production and gas/water ratio curves of multi-stage fractured horizontal wells arranged in different layers under SRV simulation. Similar to the single-fracture simulation, in the comparison of cumulative production, HBL > TPL > FGL, which were 7.165×10^7 m^3, 6.030×10^7 m^3, 2.721×10^7 m^3. Compared with the single-fracture simulation, the production of HBL increased by about 47.40%, the production of TPL increased by about 88.26%, and the production of FGL increased by only about 7.68%. Combined with the change in gas/water ratio, it was not difficult to see that HBL was still the layer with the highest production in long-term production, but the largest increase in production was in TPL, whose gas/water ratio was even close to HBL in the range of about 1300–1500 days. This shows that, when choosing the production increase method to form the reservoir transformation volume, both HBL and TPL can be used as the location of the horizontal well section, but HBL has the best production potential.

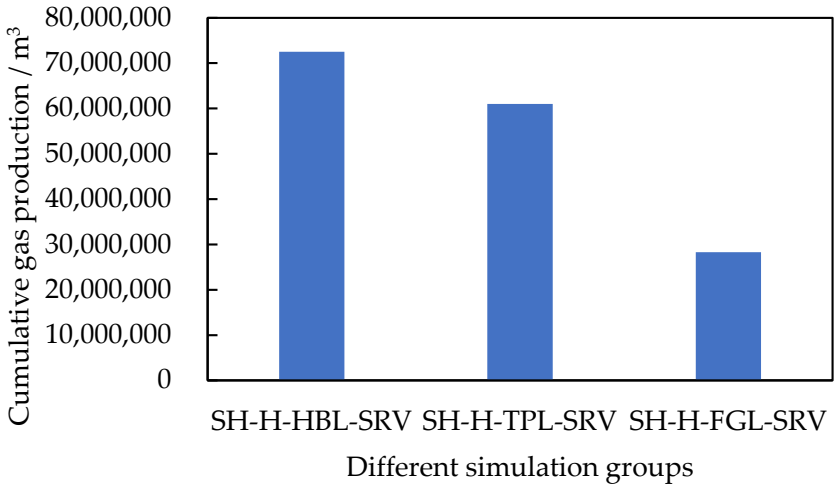

Figure 10. Cumulative gas production considering the SRV simulation approach.

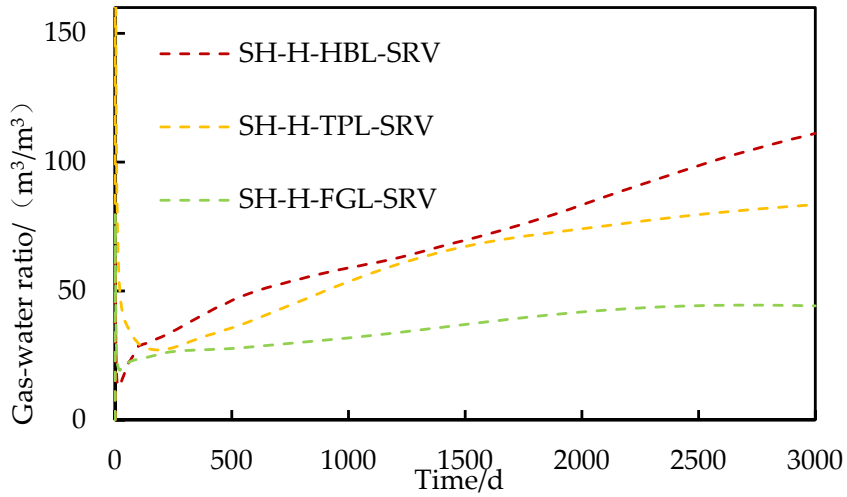

Figure 11. Gas-to-water ratio curves considering the SRV simulation approach.

4.4. Optimal Fracture Positions for Multilateral Wells

This section explores the impact of wellbore branches located in different layers on production increase in multilateral wells for fracturing production. The setting of fractures was similar to those shown in Figure 2. Three wellbore branches were set, distributed in the 7th layer (HBL), 12th layer (TPL), and 17th layer (FGL) of the model, where SH-M-HBL was a fracture set in HBL that vertically penetrated the layer where the wellbore branch was located. The settings of SH-M-TPL and SH-M-FGL were similar. The fracture conductivity was 100 × 10^{-3} μm^2·m, the fracture spacing was 80 m, the number of fractures on the branch was 3, and the FGL was 50 m.

Figures 12 and 13 show the cumulative gas production and gas/water ratio curves of different fracturing branches of multilateral wells under single-fracture simulation. The cumulative production and gas/water ratio of HBL and TPL were close, but FGL was significantly lower than the two. The cumulative production of the three simulation groups at 3000 days was 4.294 × 10^7 m^3, 4.193 × 10^7 m^3, 3.060 × 10^7 m^3, and gas/water ratios were 72.54 m^3/m^3, 69.78 m^3/m^3, and 56.30 m^3/m^3, respectively. The reason for this is that there was no hydrate in FGL. Even if the wellbore branch in this layer was fractured to promote the energy supply of the bottom layer to accelerate the decomposition of hydrates in TPL and HBL, the wellbore position did not reduce the pressure above the FGL wellbore branch, and the hydrate in this area was almost not decomposed. Therefore, the fracturing branch

of FGL in the multilateral well cannot play an additional role in increasing production. According to the conclusions in Section 3, since the multilateral well replaced part of the fractures to improve the seepage capacity, the difference between the fracturing branches located in HBL and TPL was not large and the production of SH-M-HBL and SH-M-TPL was close.

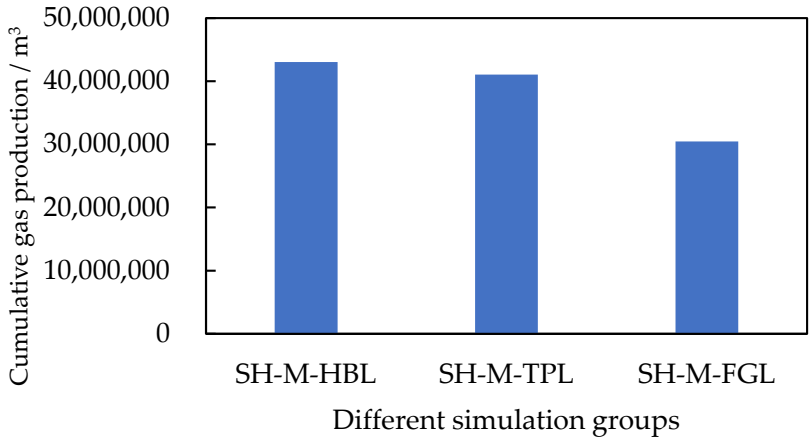

Figure 12. Cumulative gas production for the multilateral well case.

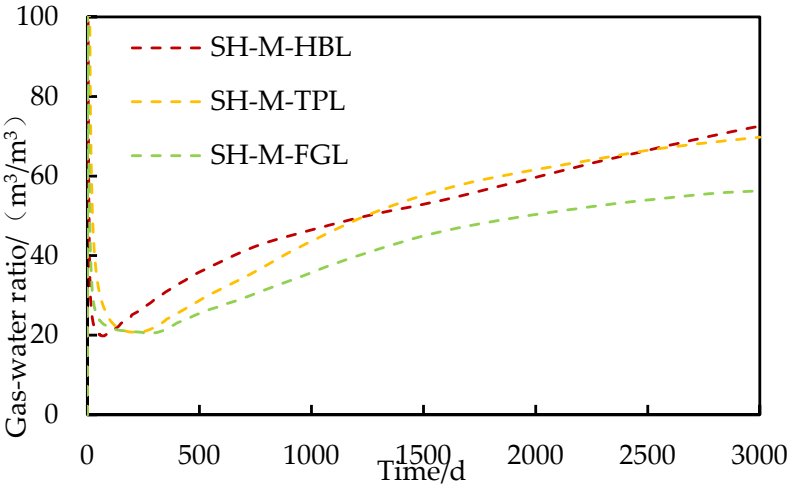

Figure 13. Gas-to-water ratio curves for the multilateral well case.

Figures 14 and 15 show the cumulative gas production and gas/water ratio curves of different fracturing branches of multilateral wells under SRV simulation. It can be seen that the gap between HBL and TPL became smaller and smaller. Compared with the single-fracture simulation, production increased by about 30–40%, and the gap with FGL was even greater. The cumulative production of SH-M-FGL-SRV was 3.106×10^7 m^3, and the production of the single-fracture simulation only increased by about 1.50%, which also shows that the fracturing branches of FGL in multilateral wells cannot play an additional role in increasing production. Even if the permeability around the fracture is improved, the production change is still small.

In the change in the gas/water ratio, the FGL was always lower than the HBL and TPL, indicating that the production efficiency of setting the fracturing branch at the FGL was the lowest. Compared with HBL and TPL, FGL showed a lower gas/water ratio, which demonstrated the lowest production efficiency for fracturing at this level. In summary, it can be judged that, whether it is a single fracture or the formation of reservoir transformation

volume, the wellbore in the FGL is not suitable for fracturing and production enhancement, while the difference between HBL and TPL is not significant.

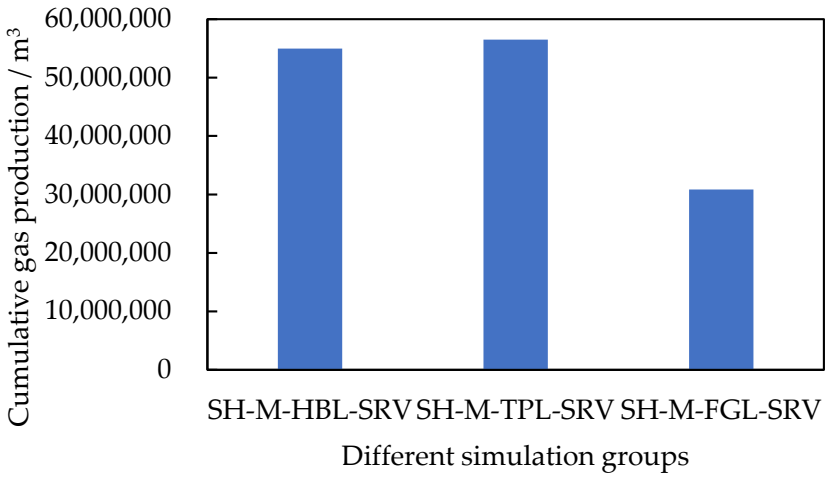

Figure 14. Cumulative gas production in the multilateral well case considering the SRV simulation approach.

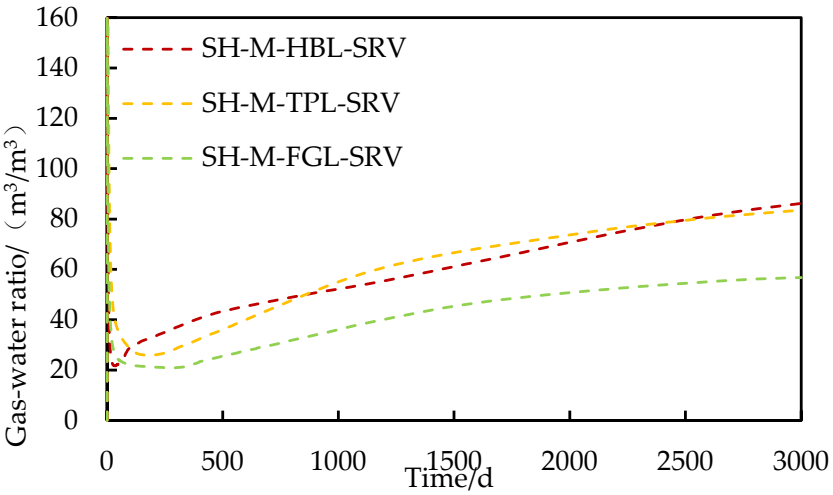

Figure 15. Gas-to-water ratio curves in the multilateral well case considering the SRV simulation approach.

This section constructs an idealized field model based on the geological data of the first hydrate test production area in the Shenhu sea area through historical matching, and explores the production increase effect of different fracture simulation methods in vertical well, horizontal well, and multilateral well fracturing production based on this model. The main conclusions are as follows: (1) In the single-fracture simulation, the production potential of vertical wells is greater when FGL is selected as the fracturing well location; however, the opposite trend is shown in horizontal wells and multilateral wells; that is, the gas production and production efficiency of FGL in horizontal wells and multilateral wells are the lowest, while the production increase effect of arranging the fracturing wellbore section at HBL is the most obvious. (2) In the simulation method considering SRV, HBL has the best production increase effect in vertical wells, horizontal wells, and multilateral wells. Among them, the production of horizontal wells is the highest. The cumulative gas production of horizontal wells in HBL simulation for 3000 days is 7.165×10^7 m^3; the production increase in TPL is the most obvious. The production of horizontal wells located in TPL is about 88.26% higher than that of single-fracture simulation under the

same conditions, but the production is lower than that of HBL. The production increase effect of FGL is the weakest. Its production volume is only 2.721×10^7 m^3. This is only about 7.68% higher than the result of the single-fracture simulation. When compared with the production of the vertical well + stimulation volume, specifically SH-V-3-SRV (2.526×10^7 m^3), the increase is merely 7.72%. With a production volume of 2.721×10^7 m^3, FGL delivers the weakest improvement. The increase equals 7.68% over the single-fracture simulation and only 7.72% compared with SH-V-3-SRV (2.526×10^7 m^3). In summary, when adopting reservoir transformation + complex structure well production increase measures, from the perspective of gas production and production efficiency, HBL in the Shenhu sea area should be considered as the first layer to be mined, followed by TPL, and arranging the wellbore in FGL has no obvious promoting effect on the decomposition and gas production of hydrates.

5. Conclusions

This study addresses the challenges and optimization strategies for the development of natural gas hydrate reservoirs, with a particular focus on enhancing production in low-permeability formations. The findings demonstrate that traditional single-extraction methods are inadequate for large-scale long-term commercial exploitation of hydrates. However, the combined application of multiple production techniques, including reservoir transformation and fracture optimization, significantly enhances production efficiency. The embedded discrete fracture model (EDFM) has proven to be an effective tool for accurately simulating the impact of fracture networks on gas production, offering valuable insights into the complex relationship between fracture geometry and reservoir conditions. Numerical simulations suggest that the production enhancement effect of HBL is the best in vertical wells, horizontal wells, and multilateral wells, with the highest production achieved in horizontal well development. The cumulative gas production over 3000 days in the HBL simulation for horizontal wells is 7.165×10^7 m^3. TPL shows the most significant improvement in production, with horizontal wells under TPL achieving about an 88.26% increase in production compared with the single-fracture simulation under the same conditions, although the production is still lower than that of HBL. The production enhancement effect in FGL is the weakest, with an increase of only about 7.68% compared with the single-fracture simulation, and only a 7.72% increase compared with the vertical well plus modified volume, i.e., SH-V-3-SRV. This study further confirms that integrating reservoir transformation measures, such as hydraulic fracturing and multi-stage production strategies, is essential for maximizing gas recovery from hydrate reservoirs. The findings provide a solid foundation for the future commercial development of natural gas hydrates, particularly in regions such as the South China Sea.

Author Contributions: Conceptualization, formal analysis, writing—original draft, supervision, project administration, funding acquisition, Q.F.; methodology, formal analysis, investigation, M.C.; data curation, supervision, review and editing, validation, W.P.; formal analysis, methodology, W.S. All authors have read and agreed to the published version of the manuscript.

Funding: This research was funded by the National Key Research and Development Program of China (No. 2021YFC2800902), the National Natural Science Funding (52474076), Director's fund of State Key Laboratory of Offshore Natural Gas Hydrates (2025), Research on Cross-Scale Phase Transition Characteristics and Numerical Simulation Methods for Depressurization Development of Natural Gas Hydrates (KJQZ-2023-2003), and Beijing Science and Technology Nova Program Project (20240484721).

Data Availability Statement: The data presented in this study are available upon request from the corresponding author.

Conflicts of Interest: Authors Qiang Fu, Mingqiang Chen, and Weixin Pang were employed by the company China National Offshore Oil Corporation. The remaining authors declare that the research was conducted in the absence of any commercial or financial relationships that could be construed as a potential conflict of interest.

References

1. Li, X.S.; Xu, C.G.; Zhang, Y.; Ruan, X.K.; Li, G.; Wang, Y. Investigation into gas production from natural gas hydrate: A review. *Appl. Energy* **2016**, *172*, 286–322. [CrossRef]
2. Zhou, S.; Wang, J.; Liang, Y. Development of China's natural gas industry in the 14th Five-Year Plan under the background of carbon neutrality. *Nat. Gas Ind.* **2021**, *41*, 171–182. [CrossRef]
3. Zhang, H.; Zhu, Y. Investigation and research on natural gas hydrate in permafrost regions of China. *Geol. Bull.* **2011**, *31*, 1809–1815. [CrossRef]
4. Zeng, F.; Wu, L.; He, Y. A review of foreign research on natural gas hydrates. *Mar. Geol. Dyn.* **2003**, *11*, 19–23. (In Chinese)
5. Sloan, E.D., Jr.; Koh, C.A.; Koh, C.A. *Clathrate Hydrates of Natural Gases*, 3rd ed.; CRC Press: Boca Raton, FL, USA, 2008.
6. Wu, N.; Zhang, H.; Yang, S.; Liang, J.; Wang, H. Preliminary study on the natural gas hydrate reservoir system in Shenhu area of South China Sea. *Nat. Gas Ind.* **2007**, *27*, 1–6. [CrossRef]
7. Myshakin, E.M.; Seol, Y.; Lin, J.-S.; Uchida, S.; Collett, T.S.; Boswell, R. Numerical simulations of depressurization-induced gas production from an interbedded turbidite gas hydrate-bearing sedimentary section in the offshore India: Site NGHP-02-16 (Area-B). *Mar. Pet. Geol.* **2018**, *108*, 619–638. [CrossRef]
8. Sun, J.; Ning, F.; Zhang, L.; Liu, T.; Peng, L.; Liu, Z.; Li, C.; Jiang, G. Numerical simulation on gas production from hydrate reservoir at the 1st offshore test site in the eastern Nankai Trough. *J. Nat. Gas Sci. Eng.* **2016**, *30*, 64–76. [CrossRef]
9. Anderson, B.; Hancock, S.; Wilson, S.; Enger, C.; Collett, T.; Boswell, R.; Hunter, R. Formation pressure testing at the Mount Elbert Gas Hydrate Stratigraphic Test Well, Alaska North Slope: Operational summary, history matching, and interpretations. *Mar. Pet. Geol.* **2011**, *28*, 478–492. [CrossRef]
10. Qin, X.; Lu, J.; Lu, H.; Qiu, H.-J.; Liang, J.-Q.; Kang, D.-J.; Zhan, L.-S.; Lu, H.-F.; Kuang, Z.-G. Coexistence of natural gas hydrate, free gas and water in the gas hydrate system in the Shenhu Area, South China Sea—ScienceDirect. *China Geol.* **2020**, *3*, 210–220.
11. Tang, X.; Chen, J.; Guo, Y.; Liang, F.; Wang, C. Review of the development status of methane hydrate development and pilot production technology. *Nat. Gas Oil* **2020**, *38*, 7–15. (In Chinese) [CrossRef]
12. Huang, M.; Wu, L.; Ning, F.; Wang, J.; Dou, X.; Zhang, L.; Liu, T.; Jiang, G. Research progress on natural gas hydrate reservoir transformation. *Nat. Gas Ind.* **2022**, *42*, 160–174.
13. Feng, Y.; Chen, L.; Suzuki, A.; Kogawa, T. Enhancement of gas production from methane hydrate reservoirs by the combination of hydraulic fracturing and depressurization method. *Energy Convers. Manag.* **2019**, *184*, 194–204. [CrossRef]
14. Chen, C.; Yang, L.; Jia, R.; Sun, Y.; Guo, W.; Chen, Y.; Li, X. Simulation study on the effect of fracturing technology on the production efficiency of natural gas hydrate. *Energies* **2017**, *10*, 1241. [CrossRef]
15. Wu, N.; Li, Y.; Wan, Y.; Sun, J.; Huang, L.; Mao, P. Prospects of the theory and technology system for increasing production of natural gas hydrate in offshore areas. *Nat. Gas Ind.* **2020**, *40*, 100–115.
16. Sun, J.; Ning, F.; Liu, T.; Liu, C.; Chen, Q.; Li, Y.; Cao, X.; Mao, P.; Zhang, L.; Jiang, G. Gas production from a silty hydrate reservoir in the South China Sea using hydraulic fracturing: A numerical simulation. *Energy Sci. Eng.* **2019**, *7*, 1106–1122. [CrossRef]
17. Meng, Y. Optimization of Parameters for Depressurization and Thermal Shock Production of Natural Gas Hydrate Under Reservoir Transformation Conditions. Master's Thesis, Jilin University, Changchun, China, 2022. (In Chinese)
18. Ruan, X.; Li, X.; Xu, C.; Zhang, Y.; Yan, K. Numerical simulation of natural gas hydrate depressurization combined with wellbore heating production. *J. Chem. Ind. Eng.* **2015**, *66*, 1544–1550. [CrossRef]
19. Zhao, E.; Hou, J.; Du, Q.; Liu, Y.; Ji, Y.; Bai, Y. Numerical modeling of gas production from methane hydrate deposits using low-frequency electrical heating assisted depressurization method. *Fuel* **2021**, *290*, 120075. [CrossRef]
20. Ye, J.; Qin, X.; Xie, W.; Lu, H.; Ma, B.; Qiu, H.; Liang, J.; Lu, J.; Kuang, Z.; Lu, C.; et al. Main progress of the second trial production of natural gas hydrate in the South China Sea. *Geol. China* **2020**, *47*, 557–568.
21. Mou, P.; Pan, J.; Wang, K.; Wei, J.; Yang, Y.; Wang, X. Influences of hydraulic fracturing on microfractures of high-rank coal under different in-situ stress conditions. *Fuel* **2020**, *287*, 119566. [CrossRef]
22. Ito, E.; Nakamura, H.; Inagaki, M. Preparation of porous carbons from cypress using super-heated steam. III. Performance in electric double layer capacitor. *TANSO* **2008**, *2008*, 8–12. [CrossRef]
23. Zhang, W.; Shi, X.; Jiang, S.; Cao, Q.; Wang, F.; Wang, Z.; Ge, Y.; Du, Y. Experimental study of hydraulic fracture initiation and propagation in highly saturated methane-hydrate-bearing sands. *J. Nat. Gas Sci. Eng.* **2020**, *79*, 103338. [CrossRef]
24. Karimi-Fard, M.; Firoozabadi, A. Numerical Simulation of Water Injection in Fractured Media Using the Discrete-Fracture Model and the Galerkin Method. *SPE Reserv. Eval. Eng.* **2003**, *6*, 117–126. [CrossRef]

25. Lee, S.H.; Lough, M.F.; Jensen, C.L. Hierarchical modeling of flow in naturally fractured formations with multiple length scales. *Water Resour. Res.* **2001**, *37*, 443–455. [CrossRef]
26. Moinfar, A.; Varavei, A.; Sepehrnoori, K.; Johns, R.T. Development of a Novel and Computationally-Efficient Discrete-Fracture Model to Study IOR Processes in Naturally Fractured Reservoirs. In Proceedings of the SPE Improved Oil Recovery Symposium, Tulsa, OK, USA, 14–18 April 2012. [CrossRef]
27. Carlson, E.S.; Latham, G.V. Naturally Fractured or Single-Porosity? The Importance of Reservoir Flow Model for Performance Assessment of Stimulated Tight Gas Wells. In Proceedings of the SPE Oklahoma City Oil and Gas Symposium/Production and Operations Symposium, Oklahoma City, OK, USA, 21–23 March 1993.
28. Karimi-Fard, M.; Firoozabadi, A. Numerical Simulation of Water Injection in 2D Fractured Media Using Discrete-Fracture Model. In Proceedings of the SPE Annual Technical Conference and Exhibition, New Orleans, LA, USA, 30 September–2 October 2001. [CrossRef]
29. Li, L.; Lee, S.H. Efficient field-scale simulation of black oil in a naturally fractured reservoir through discrete fracture networks and homogenized media. *SPE Reserv. Eval. Eng.* **2008**, *11*, 750–758.
30. Moinfar, A.; Varavei, A.; Sepehrnoori, K.; Johns, R.T. Development of a Coupled Dual Continuum and Discrete Fracture Model for the Simulation of Unconventional Reservoirs. In Proceedings of the SPE Reservoir Simulation Symposium, The Woodlands, TX, USA, 18–20 February 2013. [CrossRef]
31. Tene, M.; Bosma, S.B.M.; Al Kobaisi, M.S.; Hajibeygi, H. Projection-based Embedded Discrete Fracture Model (pEDFM). *Adv. Water Resour.* **2017**, *105*, 205–216. [CrossRef]
32. Jiang, J.; Younis, R.M. An Improved Projection-based Embedded Discrete Fracture Model (pEDFM) for Multiphase Flow in Fractured Reservoirs. *Adv. Water Resour.* **2017**, *109*, 267–289. [CrossRef]
33. Xu, J.; Qin, H.; Li, H.; Lu, C.; Li, S.; Wu, D. Enhanced gas production efficiency of class 1,2,3 hydrate reservoirs using hydraulic fracturing technique. *Energy* **2023**, *263*, 126003.
34. Xu, J.; Sun, W.; Li, H.; Li, S. Simulation of production dynamics after reservoir stimulation in hydrate reservoirs considering complex fracture morphology. *Energy Fuels* **2023**, *37*, 13866–13879. [CrossRef]
35. Gao, M.; Sun, W.; Xu, J.; Li, J. Reduced-order modeling for subsurface flow simulation in fractured reservoirs. *SPE J.* **2025**, *30*, 391–408. [CrossRef]
36. Xu, J.C.; Zhou, W.X.; Li, H.Y. Efficient production optimization for naturally fractured reservoir using EDFM. *Pet. Sci.* **2023**, *20*, 2268–2281. [CrossRef]

Disclaimer/Publisher's Note: The statements, opinions and data contained in all publications are solely those of the individual author(s) and contributor(s) and not of MDPI and/or the editor(s). MDPI and/or the editor(s) disclaim responsibility for any injury to people or property resulting from any ideas, methods, instructions or products referred to in the content.